

# High-field recovery of the undistorted triangular lattice in the frustrated metamagnet $\text{CuFeO}_2$ .

T.T.A. Lummen,<sup>1</sup> C. Strohm,<sup>2,\*</sup> H. Rakoto,<sup>3</sup> A.A. Nugroho,<sup>4</sup> and P.H.M. van Loosdrecht<sup>1,†</sup>

<sup>1</sup>*Zernike Institute for Advanced Materials, University of Groningen,  
Nijenborgh 4, 9747 AG Groningen, The Netherlands*

<sup>2</sup>*Institut Néel, CNRS et Université Joseph Fourier, BP 166, F-38042, Grenoble Cedex 9, France*

<sup>3</sup>*Laboratoire National des Champs Magnétiques Pulsés (LNCMP),  
143 avenue de Rangueil, 31400 Toulouse, France*

<sup>4</sup>*Departemen Fisika FMIPA, Institut Teknologi Bandung, Jl. Ganesa 10, Bandung 40132, Indonesia*

(Dated: July 19, 2021)

Pulsed field magnetization experiments extend the typical metamagnetic staircase of  $\text{CuFeO}_2$  up to 58 T to reveal an additional first order phase transition at high field for both the parallel and perpendicular field configuration. Virtually complete isotropic behavior is retrieved only above this transition, indicating the high-field recovery of the undistorted triangular lattice. A consistent phenomenological rationalization for the field dependence and metamagnetism crossover of the system is provided, demonstrating the importance of both spin-phonon coupling and a small field-dependent easy-axis anisotropy in accurately describing the magnetization process of  $\text{CuFeO}_2$ .

PACS numbers: 75.30.Kz, 75.10.Hk, 75.80.+q, 75.30.Gw

Metamagnetism typically refers to any material that, upon variation in the externally applied magnetic field, exhibits an abrupt change in magnetization. In general, the phase diagrams of materials undergoing field-induced magnetic transitions can be rationalized according to the degree of magnetic anisotropy in the materials<sup>1</sup>. In highly anisotropic systems, spins are effectively restricted to align (anti-)parallel to the magnetic easy-axis and magnetic transitions typically involve discontinuous spin reversals, leading to first-order type metamagnetic transitions. As for isotropic (weakly anisotropic) systems this directional restriction is relieved (strongly reduced), transitions in such materials often reflect the onset of a continuous, second order type reorientation of the local spins. Another source of exotic magnetic transitions is geometrical magnetic frustration, which occurs when a specific lattice geometry prevents the simultaneous minimization of all magnetic exchange interactions, thus introducing a high spin degeneracy<sup>2</sup>. The simultaneous occurrence of both these phenomena and the interplay between them leads to intricate, diverse and rich physics, yielding many captivating magnetic phases ranging from spin liquids and ices to multiferroic spiral phases<sup>3,4,5,6</sup>.

Here the focus is on the *delafossite* semiconductor  $\text{CuFeO}_2$ , an archetype triangular lattice antiferromagnet, in which the  $\text{Fe}^{3+}$  ions stack in hexagonal layers along the  $c$ -axis (Fig. 1(a)). In spite of the expected Heisenberg nature of the  $\text{Fe}^{3+}$  spins ( $3d^5$ ,  $S = 5/2$ ,  $L = 0$ ),  $\text{CuFeO}_2$  does not order in the noncollinear  $120^\circ$  spin configuration at low temperature. Instead, after undergoing successive phase transitions at  $T_{N1} \approx 14$  K and  $T_{N2} \approx 11$  K, lowering the symmetry from hexagonal ( $R\bar{3}m$ ) to monoclinic<sup>7,8,9</sup>, the system adopts a collinear, two-up two-down order, with moments aligned (anti)parallel along the  $c$ -axis (Fig. 1(b))<sup>10</sup>. The collinear ground state is supposedly stabilized through the strong spin-lattice coupling in  $\text{CuFeO}_2$ <sup>7,8,9,11</sup>, which induces a struc-

tural distortion through the 'spin Jahn-Teller' effect<sup>12,13</sup>. Alternatively, this scalene triangle distortion has been argued to induce an easy axis anisotropy, which was also used to account for the the observed Ising-like magnetism<sup>14,15,16</sup>. An intriguing behavior arises when  $\text{CuFeO}_2$  is subjected to an external magnetic field  $B$  below  $T_{N2}$ . With  $B \parallel c$ , the spin system has been found to successively assume a proper helical ordered ferroelectric phase, a collinear three-up two-down ordered phase, a phase with a magnetization plateau at one-third of the saturation value and a phase with steadily increasing magnetization<sup>5,15,16,17,18</sup>. Particular attention has gone to the ferroelectric helical ordered phase<sup>5,19,20,21</sup>, which has since also been stabilized in zero field through  $\text{Al}^{3+}$  or  $\text{Ga}^{3+}$  substitution<sup>22,23,24</sup>. With increasing  $B \perp c$ , the magnetization has been found to first increase steadily, then halt at a one-third plateau before resuming a (*quasi*-)linear increase at higher fields<sup>15,16</sup>. This article presents pulsed field magnetization experiments, which extend the metamagnetic staircase of  $\text{CuFeO}_2$  up to fields exceeding 58 T<sup>25</sup>. An additional high field first order phase transition is observed for both parallel and perpendicular configurations, above which virtually complete isotropic behavior is retrieved, indicating the recovery of the undistorted triangular structure. Moreover, a consistent phenomenological interpretation is provided, combining all magnetic terms deemed to be important in  $\text{CuFeO}_2$ .

As depicted in Fig. 2, the magnetization process for both  $B \parallel c$  and  $B \perp c$  shows a cascade of phase transitions, in excellent agreement with literature<sup>5,15,16,17,18,26</sup>. As  $B \parallel$  increases, the spin system successively rearranges to the helical ordered phase at  $B_{c1}^{\parallel} \simeq 7.2$  T (Fig. 1(c)) and the collinear three-up two-down phase at  $B_{c2}^{\parallel} \simeq 13.0$  T (Fig. 1(d)). Recent synchrotron x-ray-diffraction studies up to 40 T revealed the strong correlation between the spin Jahn-Teller lattice distortion and the magnetization

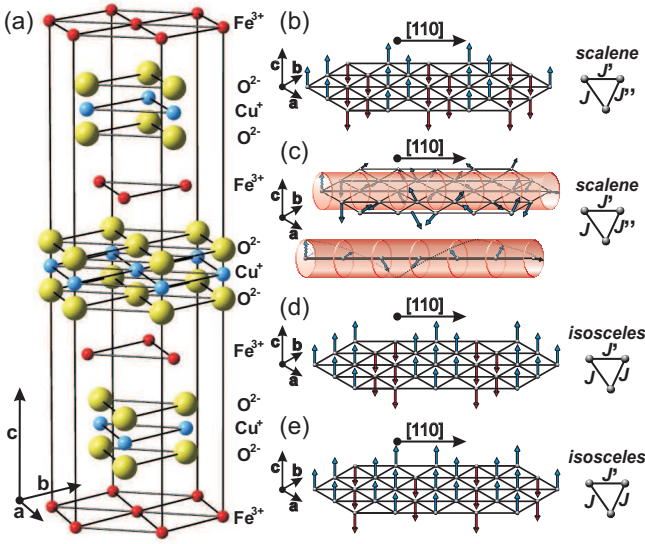


FIG. 1: (Color online) (a) Schematic crystal structure of CuFeO<sub>2</sub> ( $R\bar{3}m$ ,  $a=b=3.03\text{\AA}$ ,  $c=17.17\text{\AA}$ ). To avoid confusion, crystal directions are referred to using the hexagonal description throughout the article. (b-e) Spin structures and lattice symmetries in various field-induced phases of CuFeO<sub>2</sub> ( $B\parallel c$ ): collinear four-sublattice (4SL) phase ((b)), ferroelectric helical phase ((c)), collinear 5SL phase ((d)) and collinear 3SL phase ((e)).

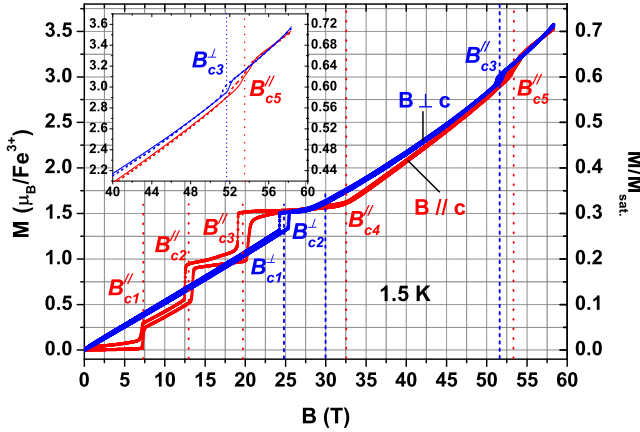


FIG. 2: (Color online) Pulsed field magnetization process for both  $B\parallel c$  (red/light gray) and  $B\perp c$  (blue/dark gray) at 1.5 K. Inset: Zoom-in on high field region.

process in CuFeO<sub>2</sub>; as  $M$  increases, the extent of the distortion decreases accordingly<sup>16,18</sup>. Since the induced magnetic anisotropy ( $D$ ) is directly coupled to the distortion, one may assume it also diminishes correspondingly with  $B$ ; exhibiting steps at first order transitions and continuously decreasing in (*quasi*)-linear phases. Moreover, at  $B_{c2}^{\parallel}$ , the symmetry of the distortion is increased, yielding a lattice of isosceles triangles<sup>9</sup>. At  $B_{c3}^{\parallel} \simeq 19.7$  T, the magnetization jumps to a plateau phase at one-third of saturation, signaling a collinear two-up one-down

order (Fig. 1(e))<sup>16,18</sup>, which is consistent with an expected nonzero  $D$  and pulsed field nuclear forward scattering experiments<sup>27</sup>. At  $B_{c4}^{\parallel} \simeq 32.4$  T, the system undergoes a second order transition, above which  $M$  starts growing continuously, indicating gradual canting of the spins away from collinearity. By extending the experimental field of view to higher fields, the persistence of this (*quasi*)-linear increase up to  $B_{c5}^{\parallel} \simeq 53.3$  T could be determined, where an additional metamagnetic transition is identified. Above this transition, up to 58.3 T,  $M$  grows steadily once more, with slightly different slope. In short, below  $B_{c4}^{\parallel}$  magnetic transitions are of first order, exhibiting significant hysteresis and large magnetization steps. From  $B_{c4}^{\parallel}$  on (second order transition),  $M$  mostly increases continuously with  $B^{\parallel}$ , and magnetization plateaus are absent. In terms of metamagnetism, this corresponds to a crossover from a highly anisotropic regime (with abrupt spin flips) to a weakly anisotropic regime (continuous spin reorientation), which is in line with the notion of progressive symmetry increase and thus magnetic anisotropy reduction upon increasing  $B$ .

For  $B\perp c$ , the magnetization process is quite different. Starting from the zero-field collinear two-up two-down phase,  $M$  shows a steady increase up to  $B_{c1}^{\perp} \simeq 24.8$  T, where a first order transition brings the system in a plateau phase at one-third of saturation, implying a three sublattice (3SL) structure. Above  $B_{c2}^{\perp} \simeq 30.0$  T, the system exhibits a steady increase of  $M$  after undergoing a second order phase transition, indicating a continuous spin reorientation. The data in Fig. 2 show this behavior persists up to  $B_{c3}^{\perp} \simeq 51.6$  T where the system undergoes an additional first order transition, similar to that at  $B_{c5}^{\parallel}$  for  $B\parallel c$ . Contrary to previous claims<sup>16</sup>, the behavior clearly remains anisotropic up to these transitions. Though left unaddressed, a corresponding feature can also be observed around 52 T in the ( $dM/dB$ ) vs.  $B$  data previously recorded in a single turn coil measurement up to 100 T (8 K)<sup>26</sup>. At fields above both these transitions,  $M$  shows virtually isotropic behavior, growing (*quasi*)-linearly up to 58.3 T. This absence of anisotropy suggests a full symmetry recovery and thus retrieval of the undistorted triangular lattice at these fields.

To elucidate the nature of the high field spin structures, we introduce a simple classical spin model for a single triangular sheet, which includes the primary terms in the spin Hamiltonian:

$$H = -g\mu_B \cdot \sum_i \mathbf{S}_i + \sum_{i,j} J_{ij} \mathbf{S}_i \cdot \mathbf{S}_j - \sum_{\langle i,j \rangle} b J_{ij} (\mathbf{S}_i \cdot \mathbf{S}_j)^2 - D(B) \sum_i S_{iz}^2, \quad (1)$$

where  $J_{ij}$  is the exchange coupling between sites  $i$  and  $j$ ,  $b$  is an effective (nearest-neighbor only) biquadratic interaction originating from the spin-lattice coupling (bond-phonon model)<sup>3,28</sup> and  $D(B)$  is the anisotropy constant ( $> 0$  for an easy-axis along  $z$ ). The first (Zeeman) and

last (anisotropy) terms sum over all sites  $i$  in the magnetic unit cell, while the summation in the exchange and biquadratic terms includes all interactions within that unit cell. The high field magnetization process is qualitatively similar for both field configurations; first the spin system exhibits a one-third magnetization plateau, implying a three sublattice (3SL) structure, after which  $M$  starts increasing steadily, indicating a continuous re-orientation of the 3SL spins. To capture this magnetic behavior, we thus study the spin Hamiltonian of the 3SL structure on a single sheet. As the lattice distortion persists up to at least 40 T for both field configurations<sup>16</sup>, a nonzero  $D$  may be expected up to these fields. Having three inequivalent spins, there are three unique first- ( $J$ ), second- ( $J^\dagger$ ) and third-neighbor ( $J^\ddagger$ ) couplings per spin in one magnetic unit cell (Fig. 3(a)). The Hamiltonian becomes (using  $g = 2$ ,  $\mathbf{S}_i = \mathbf{e}_i S$  (unit vector  $\mathbf{e}$ , classical spins) and  $p_{ij} = \mathbf{e}_i \cdot \mathbf{e}_j$ ):

$$H = -2\mu_B \mathbf{S} \mathbf{B} \cdot \sum_i \mathbf{e}_i + CS^2(p_{12} + p_{13} + p_{23}) + 9J^\dagger S^2 - GS^4(p_{12}^2 + p_{13}^2 + p_{23}^2) - D(B)S^2 \sum_i e_{i,z}^2, \quad (2)$$

where the exchange constant  $C = (3J + 3J^\dagger)$  and the spin-lattice constant  $G = 3bJ$ . The anisotropy  $D(B)$  is approximated to be 'anti-proportional' to  $M(B)$ ; as  $M$  approaches saturation,  $D$  vanishes accordingly. Note that the inclusion of further neighbor interactions has only a trivial effect; the third neighbor interactions merely add to  $C$ , while the second neighbor interactions only shift the total energy as a whole.

We determined the spin directions  $\mathbf{e}_1$ ,  $\mathbf{e}_2$  and  $\mathbf{e}_3$  corre-

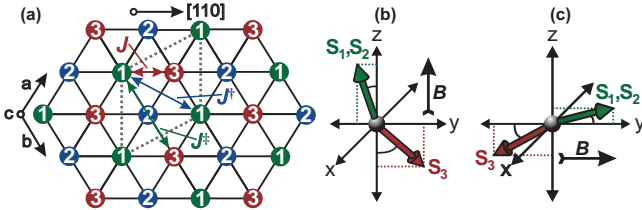


FIG. 3: (Color online) (a) Exchange interactions in the 3SL structure on the 2D isosceles triangle lattice. Minimum energy solutions of eq. 2 for a 3SL structure with finite  $D$  are depicted for  $B \parallel c$  ((b)) and  $B \perp c$  ((c)).

sponding to the minimum energy per unit cell at a given field  $\mathbf{B}$  by performing numerical minimization of eq. 2. In examining the corresponding simulated magnetization curves, one finds that having both the anisotropy constant  $D(B)$  and the spin-lattice constant  $G$  nonzero is a prerequisite for good qualitative agreement with experiment; with  $D = 0$  the magnetization process becomes isotropic, while a nonzero  $G$  is required to stabilize a magnetization plateau for  $B \perp c$ . Matching the simulated magnetization curves with experiment yields estimates for the exchange, anisotropy and spin-lattice constants of  $C = 1.32$  meV,  $D(25\text{T}) = 0.021$  meV (plateau) and

$G = 0.0074$  meV, respectively, the resulting curves are plotted in Fig. 4. Taking only first-neighbor interactions, we can estimate  $JS^2$  as  $\sim 2.76$  meV (32.0 K) and  $DS$  (at 25T) as  $\sim 0.052$  meV (0.6 K), in line with previous estimates<sup>11,14,15</sup>. For  $GS^4$  we estimate  $\sim 0.29$  meV (3.4 K), yielding a dimensionless biquadratic coupling  $b$  of  $\sim 0.0056$  (compared to  $\sim 0.008$  using estimates from ref. 11). With these parameters the simulations are in striking agreement with experiment. The spin-lattice interaction  $G$  (non-directional) stabilizes the one-third magnetization plateau in both configurations, while the directional anisotropy interaction  $D$  widens the plateau for  $B \parallel c$  and narrows it for  $B \perp c$ , leading to the difference in plateau-widths and above-plateau increase of  $M$ . Moreover, a nonzero  $G$  also induces a positive  $\partial^2 M / \partial B^2$  in the latter, as is observed in experiment.

According to the minimum energy solution the three

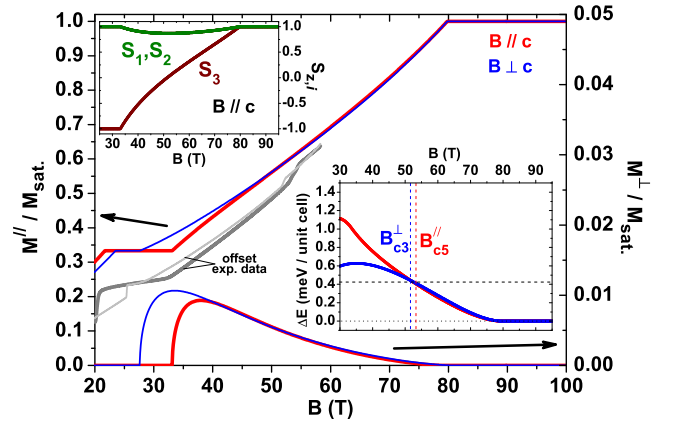


FIG. 4: (Color online) Simulated magnetization process (eq. 2) in  $\text{CuFeO}_2$  for both  $B \parallel c$  (thick, red) and  $B \perp c$  (thin, blue).  $M$  is plotted in the both the field direction (left axis,  $M^{\parallel}$ ) and the plane perpendicular to  $B$  (right axis,  $M^{\perp}$ ). Thick dark (thin light) grey lines depict offset experimental data for  $B \parallel c$  ( $B \perp c$ ). Upper inset: field-dependence of z-components of individual spins for  $B \parallel c$ . Lower inset: estimated magnetic energy gain w.r.t. isotropic spin structure (see text).

spins evolve as follows for  $B \parallel c$ : below  $B_{c4}^{\parallel}$ , the system is in the collinear 3SL state, with two spins ( $S_1$  and  $S_2$ ) parallel to  $B^{\parallel}$ , and one ( $S_3$ ) antiparallel. As depicted in the upper inset of Fig. 4, from  $B_{c4}^{\parallel}$  on, the 'down' spin starts continuously tilting from 'down' to 'up', thereby increasing  $M$ . In optimizing the overall magnetic energy, the two 'up' spins respond by first moving slightly away from the  $c$ -axis in the opposite direction, before gradually returning after the 'down' spin has passed the basal plane. Due to the finite  $D$  and  $G$ , the two 'up' spins remain collinear (Fig. 3(b)) and the system also acquires a small in-plane magnetization, which quickly grows and slowly decreases with  $B^{\parallel}$  above  $B_{c4}^{\parallel}$  (Fig. 4). Although the process is qualitatively similar for  $B \perp c$  (Fig. 3(c)), quantitatively it differs slightly due to the orthogonality of the field- and anisotropy directions in this case.

The model does not directly account for the additionally observed high field transitions; it predicts continuous evolution toward full saturation. However, the model assumes a distortion-induced finite anisotropy  $D(B)$ , while the associated elastic energy cost is not included in the all-magnetic Hamiltonian. The amount of magnetic energy the system gains upon having a distortion (and thus finite  $D$ ) can be approximated by taking the difference between the energy of an isotropic spin configuration (e.g. a *canted*  $120^\circ$  configuration, with all three spins tilted away from the field-direction, while their projections in the orthogonal plane keep mutual  $120^\circ$  angles) and the minimum energy solution of eq. 2 (lower inset of Fig. 4). The first order transitions at  $B_{c5}^{\parallel}$  and  $B_{c3}^{\perp}$  can then be identified as the point where the magnetic energy gain no longer outweighs the elastic cost of the distortion, upon which the system reverts to the undistorted triangular lattice, which is corroborated by the observed isotropy in  $M$  above  $B_{c5}^{\parallel}$  (Fig. 2). We note the estimated magnetic energy gain at this point is  $\sim 0.42$  meV per unit cell (3 spins), which is approximately the temperature scale of the experimental data ( $3kT$  at 1.5 K is  $\sim 0.39$  meV). This is consistent with the fact that  $B_{c5}^{\parallel}$  and  $B_{c3}^{\perp}$  are observed to shift toward lower fields with increasing temperature. For an isotropic lattice above  $B_{c5}^{\parallel}$ , the model predicts a degenerate set of spin structures, among which the aforementioned *canted*  $120^\circ$  structure.

Despite its satisfactory and intuitive results, our simple model has its limitations. Though the low field collinear phases can be modeled using eq. 1, being a phenomenological model meant to describe the high field phases, it does not capture the complex helical ferroelectric phase.

A full quantitative description of  $\text{CuFeO}_2$  would require the inclusion of finite temperature, three dimensionality (recent work showed the significance of interplane couplings<sup>14,15,29,30</sup>), a more refined phonon model, quantum spins and possibly other interactions<sup>31</sup>.

Concluding, through pulsed field magnetization experiments, the metamagnetic staircase characteristic of  $\text{CuFeO}_2$  was extended to up to 58.3 T, revealing an additional first order phase transition for both magnetic field configurations, which is proposed to be due to a reversed spin Jahn Teller transition. Above this transition, virtually complete isotropic behavior is retrieved. A highly consistent phenomenological rationalization for the magnetization process in both magnetic field configurations is developed, combining for the first time all magnetic terms deemed of importance in  $\text{CuFeO}_2$ . Numerical simulations based on the corresponding classical model prove the pertinence of both spin-lattice and field-dependent anisotropy interactions in  $\text{CuFeO}_2$ . Combined with the magnetization measurements, a recovery of the undistorted triangular lattice structure is anticipated at high fields. The underlying intuitive concept of progressive symmetry increase as the degree of frustration in spin Jahn-Teller distorted systems diminishes is rather universal, as it relies solely on energy arguments. Indeed, a similar high field transition has been observed recently in  $\text{HgCr}_2\text{O}_4$  and corresponding transitions may be expected in related spinel systems<sup>6</sup>.

The authors would like to thank F. de Haan and D. Maillard for technical support. Financial support from the Agence Nationale de Recherche under contract NT05-4.42463 is gratefully acknowledged.

\* Current address: European Synchrotron Radiation Facility (ESRF) - P.O. Box 220, 38043 Grenoble, France

† Electronic address: P.H.M.van.Loosdrecht@rug.nl

<sup>1</sup> E. Strykowski and N. Giordano, Adv. Phys. **26**, 487 (1977).

<sup>2</sup> A. P. Ramirez, Annu. Rev. Mater. Sci. **24**, 453 (1994).

<sup>3</sup> K. Penc, N. Shannon, and H. Shiba, Phys. Rev. Lett. **93**, 197203 (2004).

<sup>4</sup> J. E. Greedan, J. Alloys Compd. **408-412**, 444 (2006).

<sup>5</sup> T. Kimura, J. C. Lashley, and A. P. Ramirez, Phys. Rev. B **73**, 220401(R) (2006).

<sup>6</sup> H. Ueda, H. Mitamura, T. Goto, and Y. Ueda, Phys. Rev. B **73**, 094415 (2006).

<sup>7</sup> N. Terada, S. Mitsuda, H. Ohsumi, and K. Tajima, J. Phys. Soc. Jpn. **75**, 023602 (2006).

<sup>8</sup> F. Ye, Y. Ren, Q. Huang, J. A. Fernandez-Baca, P. Dai, J. W. Lynn, and T. Kimura, Phys. Rev. B **73**, 220404(R) (2006).

<sup>9</sup> N. Terada, Y. Tanaka, Y. Tabata, K. Katsumata, A. Kikkawa, and S. Mitsuda, J. Phys. Soc. Jpn. **75**, 113702 (2006).

<sup>10</sup> M. Mekata, N. Yaguchi, T. Takagi, S. Mitsuda, and H. Yoshizawa, J. Magn. Magn. Mater. **104-107**, 823 (1992).

<sup>11</sup> F. Wang and A. Vishwanath, Phys. Rev. Lett. **100**, 077201

(2008).

<sup>12</sup> Y. Yamashita and K. Ueda, Phys. Rev. Lett. **85**, 4960 (2000).

<sup>13</sup> O. Tchernyshyov, R. Moessner, and S. L. Sondhi, Phys. Rev. B **66**, 064403 (2002).

<sup>14</sup> F. Ye, J. A. Fernandez-Baca, R. S. Fishman, Y. Ren, H. J. Kang, Y. Qiu, and T. Kimura, Phys. Rev. Lett. **99**, 157201 (2007).

<sup>15</sup> O. A. Petrenko, M. R. Lees, G. Balakrishnan, S. de Brion, and G. Chouteau, J. Phys.: Condens. Matter **17**, 2741 (2005).

<sup>16</sup> N. Terada, Y. Narumi, Y. Sawai, K. Katsumata, U. Staub, Y. Tanaka, A. Kikkawa, T. Fukui, K. Kindo, T. Yamamoto, et al., Phys. Rev. B **75**, 224411 (2007).

<sup>17</sup> S. Mitsuda, M. Mase, T. Uno, H. Kitazawa, and H. A. Katori, J. Phys. Soc. Jpn. **69**, 33 (2000).

<sup>18</sup> N. Terada, Y. Namuri, K. Katsumata, T. Yamamoto, U. Staub, K. Kindo, M. Hagiwara, Y. Tanaka, A. Kikkawa, H. Toyokawa, et al., Phys. Rev. B **74**, 180404(R) (2006).

<sup>19</sup> T. Arima, J. Phys. Soc. Jpn. **76**, 073702 (2007).

<sup>20</sup> T. Nakajima, S. Mitsuda, S. Kanetsuki, K. Prokes, A. Podlesnyak, H. Kimura, and Y. Noda, J. Phys. Soc. Jpn. **76**, 043709 (2007).

<sup>21</sup> T. Nakajima, S. Mitsuda, S. Kanetsuki, K. Tanaka, K. Fu-



- jii, N. Terada, M. Soda, M. Matsuura, and K. Hirota, Phys. Rev. B **77**, 052401 (2008).
- <sup>22</sup> S. Seki, Y. Yamasaki, Y. Shiomi, S. Iguchi, Y. Onose, and Y. Tokura, Phys. Rev. B **75**, 100403(R) (2007).
- <sup>23</sup> S. Kanetsuki, S. Mitsuda, T. Nakajima, D. Anazawa, H. A. Katori, and K. Prokes, J. Phys.: Condens. Matter **19**, 145244 (2007).
- <sup>24</sup> N. Terada, T. Nakajima, S. Mitsuda, H. Kitazawa, K. Kaneko, and N. Metoki, Phys. Rev. B **78**, 014101 (2008).
- <sup>25</sup> Samples were prepared from an oriented single crystal grown using the floating zone technique.
- <sup>26</sup> Y. Ajiro, T. Asano, T. Takagi, M. Mekata, H. A. Katori, and T. Goto, Physica B **201**, 71 (1994).
- <sup>27</sup> C. Strohm, unpublished.
- <sup>28</sup> D. L. Bergman, R. Shindou, G. A. Fiete, and L. Balents, Phys. Rev. B **74**, 134409 (2006).
- <sup>29</sup> N. Terada, S. Mitsuda, T. Fujii, and D. Petitgrand, J. Phys.: Condens. Matter **19**, 145241 (2007).
- <sup>30</sup> R. S. Fishman, F. Ye, J. A. Fernandez-Baca, J. T. Haraldsen, and T. Kimura, Phys. Rev. B **78**, 140407(R) (2008).
- <sup>31</sup> M. L. Plumer, Phys. Rev. B **78**, 094402 (2008).